Lightweight cement pastes with hollow glass microspheres: Analytical estimation of elastic parameters

Christian Marcelo Martín, Siavash Ghabezloo, Teresa María Piqué, Jean-Michel Pereira, Diego Guillermo Manzanal

Cement and Concrete Research 172 (2023) 107200

Contents lists available at ScienceDirect

Cement and Concrete Research

journal homepage: www.elsevier.com/locate/cemconres

Lightweight cement pastes with hollow glass microspheres: Analytical estimation of elastic parameters

Christian Marcelo Martín [a,b], Siavash Ghabezloo [a], Teresa María Piqué [c,e], Jean-Michel Pereira [a], Diego Guillermo Manzanal [d,*]

[a] Navier, Ecole des Ponts, Univ Gustave Eiffel, CNRS, Marne-la-Vallee, France
[b] Facultad de Ingenieria, Universidad Nacional de la Patagonia San Juan Bosco, Comodoro Rivadavia, Argentina
[c] YPF Tecnologia S.A., Buenos Aires, Argentina
[d] ETSI de Caminos, Canales y Puertos, Universidad Politecnica de Madrid, Madrid, Spain
[e] CONICET, Ciudad Autonoma de Buenos Aires, Buenos Aires, Argentina

ARTICLE INFO

Keywords:
Lightweight cement
Hollow glass microspheres
Deep well cement
Micromechanics
Elastic parameters
Imperfect interface

ABSTRACT

An analytical model is presented for estimation of the elastic parameters of lightweight cement pastes with hollow glass microspheres (HGMS). The microspheres consist of a siliceous spherical outer shell filled with gas, providing a density modification agent for the cement paste. The obtained lightweight cement paste is used for cementing deep wells where it is necessary to guarantee the integrity of the cement sheath to avoid fluid migration, contain the rock mass and protect the casing. The proposed micromechanical model, compared to other alternatives, results in an easy-to-use approach for obtaining an estimation of the elastic parameters of the HGMS lightweight cement. The elastic parameters are necessary for the design of the cement sheath and the analysis of its performances. The model input parameters are the elastic parameters of the cement matrix and the microspheres, as well as microspheres dimensions and volume fraction, which are easy to obtain. The model predictions are compared to experimentally evaluated elastic parameters of lightweight cement pastes. A good compatibility between predictions and experimental data is obtained, even when assuming a perfectly bounded interface between the microspheres and the cement matrix.The model also permits to take into account an imperfect interface between the microspheres and the cement matrix improving the model predictions with respect to the experimental results. The model presents an engineering tool to design lightweight cement slurries with hollow microspheres and to estimate their mechanical contribution to a cement sheath for drilling operations.

1. Introduction

In the industries of geothermal energy, oil production, CO_2 geological storage, among others, in which it is necessary to build deep wells, it is important to accomplish adequate well cementing to satisfy the required zonal isolation, formation support, and casing protection. During the placement operations, the cement slurry should meet the same density requirements as the drilling mud to ensure sufficient pressure on formation, high enough to prevent excessive failure zones, and low enough to avoid fracturing and fluid loss. In some situations, particularly in rock formations with low fracture gradients, there is a need to use lightweight cement, which permits applying a lower pressure gradient on the formation [1]. There are a variety of solutions to obtain lightweight and ultra-lightweight cement slurries, among which one can mention the use of water extenders, foam cement, or lightweight materials [2,3]. Water extenders are those materials that, when added to the slurry formulation, allow the incorporation of a higher quantity of water without severely affecting the properties of the hardened paste. Foamed cement, obtained via nitrogen injection, contains nitrogen micro-bubbles which let the slurry reach a low specific weight [4]. Lightweight materials are used as cement replacement, and since their specific weight is smaller than that of cement, the specific weight of the slurry is reduced. Depending on the lightweight material used, the final properties of the hardened cement paste will vary. Indeed, hollow glass microspheres (HGMS) are particularly interesting among different lightweight materials. This material has a very low specific weight, while it has a crush strength reaching 200 MPa. It permits to obtain lightweight cement slurries without affecting the final cement paste's compressive strength [5]. Al-Yami et al. [6] compare the solution of multistage cementing with traditional cement slurries and

* Corresponding author.
E-mail address: d.manzanal@upm.es (D.G. Manzanal).

https://doi.org/10.1016/j.cemconres.2023.107200
Received 18 November 2022; Received in revised form 17 April 2023; Accepted 16 May 2023
Available online 17 June 2023

HGMS lightweight cement slurries. The equivalent circulating density – and thus the lower circulation loss – achieved with HGMS cement slurries is sufficiently low to avoid the technical difficulties related to the multistage method. Moreover, the applicability of HGMS in the deep well cementing industry is not as difficult as other possible solutions [3]. Considering these advantages, the work presented in this paper focuses on lightweight cement pastes prepared with HGMS and, more particularly, on estimating their elastic parameters.

To design an efficient cementing in a deep well, compressive strength is not the only important material property of the cement paste. The elastic parameters are also of great importance. The development of stresses in the cement sheath in interaction with the surrounding materials, i.e., rock formation and casing, is directly dependent on its elastic properties. Under the solicitations due to the creeping or drainage of the rock formation, a cement sheath with lower elastic moduli develops lower stress levels. It is, therefore, less prone to risks related to the failure or development of plastic strains. Similarly, the thermo-mechanical stresses developed in the cement sheath following the temperature changes in the well, e.g., during mud circulation or thermal stimulation, are less intense for the cement pastes with lower elastic moduli. Using cement pastes with adequate elastic moduli seems to have also some advantages during the perforation operations [7–9]. These perforations are done with explosive charges on the casing and the cement sheath, to begin with the oil production. This activity is aimed at only affecting the intended reduced zone but, depending on the hardened cement paste properties, this could not always be the actual case. It is important to have a hardened cement paste with high toughness and low elastic moduli to reduce crack propagation.

It is, therefore, essential to have a good knowledge of the elastic parameters of the cement paste and, in this paper's particular case, the ones prepared based on HGMS. The classical and the most usual way of evaluating these parameters is by performing laboratory experiments on prepared cement paste samples. In addition to these methods, which need some experimental work and time for the preparation and maturation of the samples, it is interesting to develop alternative analytical or empirical methods permitting to estimate these properties based on some basic information on the mix design and used materials. The empirical relations can be obtained by performing a significant number of experiments with various formulations and different materials and then trying to find mathematical relations between the elastic parameters of the paste and other parameters of the slurry, e.g., water to cement ratio (w/c), HGMS fraction, etc. It is clear that this method, though interesting, is quite time-consuming and of limited applicability as the evaluated relations are limited to the tested slurries. An alternative solution can be found in micromechanical modeling and homogenization techniques [10,11]. They consist of a mathematical framework permitting to have an estimation of the macro-scale mechanical properties of a micro-heterogeneous material by knowing its phase composition in terms of volume fractions, the individual mechanical properties, shape and orientation of each microstructure phase and the interactions between phases. These methods have been previously successfully applied to cement-based materials for the evaluation of the macro-scale properties and studying the effects of the hydration progress, w/c ratio, various additives, clinker composition, etc. [12–18]. Micromechanical modeling is applied here to provide a relatively easy-to-use analytical method for estimating the elastic parameters of the lightweight cement paste prepared with HGMS, based on some basic information like the cement matrix elastic parameters, HGMS volume fraction, thickness, and diameter. It should be emphasized that the estimation of the elastic parameters of the HGMS cement paste in this paper is based on existing micromechanical models proposed originally by Hervé and Zaoui [19], for the model with perfect interfaces, and Ghabezloo [20], for the one with imperfect interfaces. The contribution of this paper is the application of these models to HGMS lightweight cement pastes.

The paper is organized into six sections. After this introduction, Section 2 is focused on presenting the lightweight cement pastes prepared using HGMS. It is followed by Section 3, which presents the theoretical framework and model equations. For simplicity, only the main equations are presented in this section, but a more detailed mathematical development of the theoretical framework is presented in the appendix. Section 4 is dedicated to some parametric and sensitivity studies using the proposed model to show the influence of different parameters on the elastic properties of the paste. The model is then verified in Section 5 based on some application examples by comparison of its predictions with experimental results. Finally, Section 6 is dedicated to presenting some conclusions and perspectives.

2. HGMS lightweight cement

HGMS are manufactured from soda-lime borosilicate glass, with silicon dioxide (SiO_2) being their principal component (60%–87%) [3,21]. Fig. 1 shows a Scanning Electron Microscopy (SEM) image of HGMS in which the spherical shape of the outer glass shell can be distinguished. Fig. 2 shows a SEM image of a broken HGMS where the small thickness of the outer shell can be appreciated. Given this, the volume fraction of the glass forming the outer shell results much smaller than the volume fraction of the interior void space. The particles' size varies between 20 and 70 μm. HGMS are thermally stable up to 600 °C, have low densities that range from 100 to 800 kg/m^3, and can withstand high compressive stresses before breaking, leading to strength values ranging from 20 to 200 MPa [4]. A decrease in HGMS's strength is observed for larger particle sizes and lower densities. These relatively low densities and large strengths imply that HGMS can be used to obtain lightweight cement pastes with satisfactory mechanical properties [3].

Compared to other solutions for obtaining lightweight cement pastes (higher w/c ratios, foamed cement, etc.), the use of HGMS presents various advantages conferred by their properties. Indeed, lightweight cement pastes obtained by other means generally yield lower compressive strength and greater interconnected porosity than a cement paste with HGMS [3], leading to mechanical and transport properties of the cement that might not guarantee the intended zonal isolation, formation support and casing protection. HGMS admixture was first used in a low fracture gradient offshore well in the Gulf of Mexico in 1980 [22]. In this first field application, HGMS were added to the mixture with a dosage of 27% by weight of cement to achieve a density of 1115 kg/m^3 with adequate mechanical properties.

After this first application, much research has been done with different approaches to optimize the HGMS content in cement pastes [23–26]. Many properties of fresh and hardened cement pastes are affected by this admixture, such as density, fluidity, water segregation, compressive strength, and elastic properties, among others. In these research works, it was found that the influence of HGMS on the mechanical properties of cement pastes is related to the replacement/addition percentage, the HGMS's strength and HGMS's density. It shall be mentioned that HGMS's strength and density are related since a higher density means a thicker outer shell and, therefore, a higher strength. On the one hand, it was found that replacement/addition percentage was more important than HGMS's strength. Regardless of the HGMS's strength, increasing the addition percentage by weight of cement implies a decrease in the mechanical properties of the hardened cement paste. On the other hand, for identical addition percentages, the cement paste with the HGMS of higher strength yields higher mechanical properties.

In addition, in some previous research, the chemical compatibility between HGMS and cement was studied [21]. It was found that HGMS act as nucleation agent for cement hydration products. This means that the addition of HGMS enhances to some extent, cement hydration, which was verified by isothermal calorimetry and thermogravimetric tests. In addition, HGMS were shown to present pozzolanic activity by the modified Chapelle test, the strength activity index and the

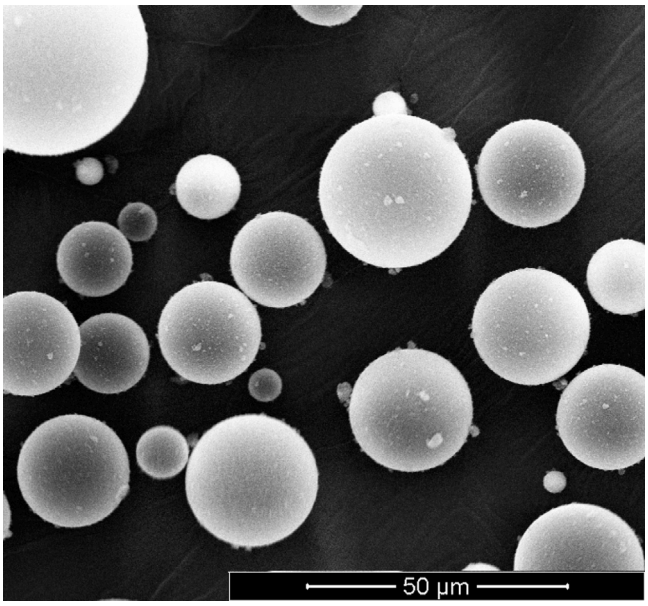

Fig. 1. Scanning Electron Microscopy image of HGMS.

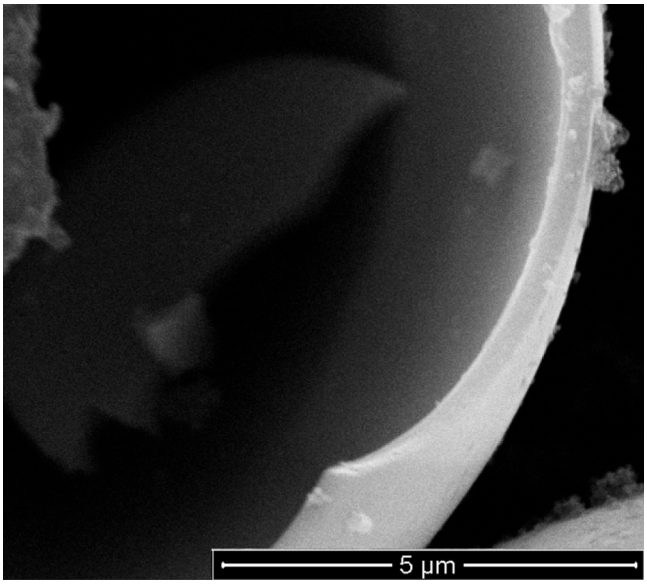

Fig. 2. Scanning Electron Microscopy image of broken HGMS.

portlandite (CH) content measured by thermogravimetric analysis at different curing ages. Fig. 3 shows a SEM image of a cement paste modified with HGMS at 28 days of curing, where cement hydration products forming around HGMS can be seen, which further verifies the compatibility between these two materials.

3. Model framework

The aim of classical homogenization method is to replace an actual heterogeneous complex body by a fictitious homogeneous one that behaves macroscopically in the same way. The principles and main equations of this framework are presented briefly in Appendix A.1. In the current section, only the main equations needed for the particular studied application are presented in scalar form. The homogenization equations are developed for the REV (Representative Elementary Volume) of a heterogeneous material which is composed of n different

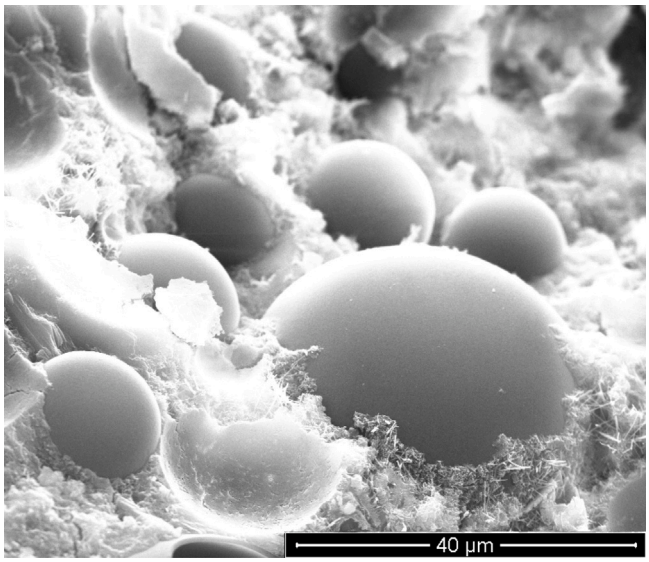

Fig. 3. Scanning Electron Microscopy image of cement paste with HGMS.

phases, each phase k having a volume fraction f_k. In the case of isotropy of the solid phases, the elastic bulk and shear moduli of a phase k are represented by k_k and g_k, respectively. Still, in the isotropic case, the homogenized macro-scale bulk and shear moduli of the material can be evaluated by the following relations (see derivation in Appendix A.1):

$$K^{\text{hom}} = \sum_{k=1}^{n} f_k\, k_k\, A_k^v \quad ; \quad G^{\text{hom}} = \sum_{k=1}^{n} f_k\, g_k\, A_k^d \tag{1}$$

Eq. (1) shows that the effective elastic moduli are equivalent to some weighted average of the elastic moduli of the constituents. The coefficients A_k^v and A_k^d are volumetric and deviatoric strain localization coefficients of each microstructure phase which play the role of weighting factors. These coefficients depend on the elastic properties of each phase and of the surrounding matrix, as well as the geometrical properties of the concerned phase. For an elastic inclusion of ellipsoidal geometry perfectly embedded in a reference elastic medium, the strain localization coefficients can be evaluated based on Eshelby's solution [27]. For the more complex geometry involved in HGMS cement a solution developed by Hervé and Zaoui [19] and Ghabezloo [20] will be adapted in the following part to evaluate the strain localization coefficients.

3.1. Basic assumptions and choice of REV

The development of the micromechanical model for the HGMS cement requires first the definition of an adequate REV to represent the microstructure of the material. Based on the SEM images, the considered REV for the HGMS cement is presented schematically in Fig. 4. It consists of HGMS inclusions embedded in a cement paste matrix. This choice of REV assumes the scale separation between the cement matrix and the HGMS inclusions. Nevertheless, one may notice that this condition is not rigorously satisfied, as the size of the unhydrated clinker grains in the cement matrix, a few tens of micrometers, is comparable to the size of HGMS. From this viewpoint, a potentially more robust choice of REV would be a multi-scale model similar to the ones used by Königsberger et al. [28] or Ghabezloo [15] in which the HGMS can be considered in the same scale as the clinker grains. However, considering the fact that the model in this paper is applied to hardened cement pastes in which the clinker grains are of relatively low volume fraction and smaller size, the assumption of scale separation between the cement matrix and HGMS does not

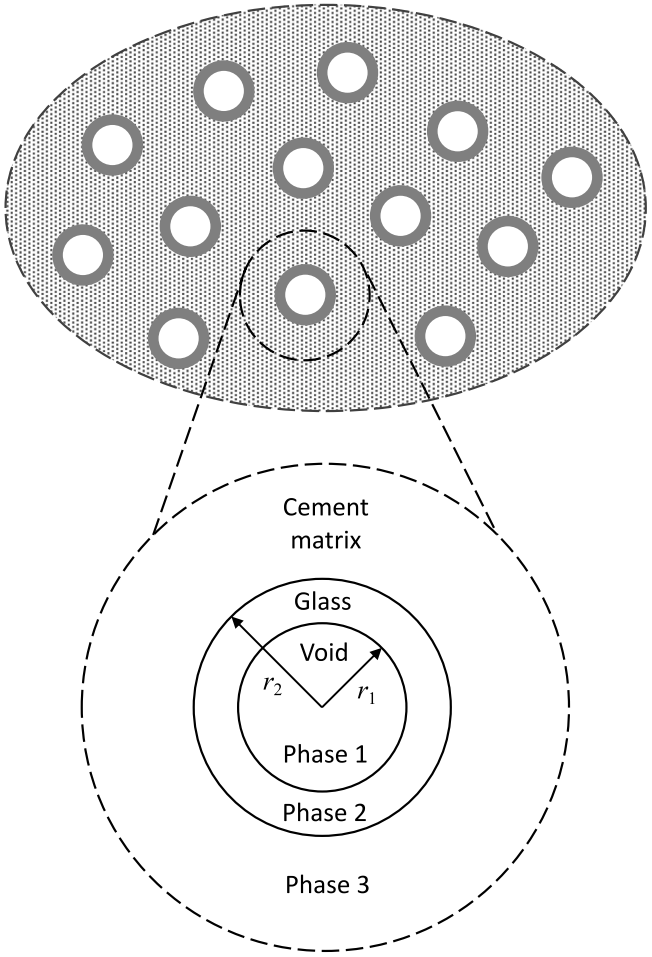

Fig. 4. Top: Schematic representation of the REV of the lightweight cement paste based on HGMS, Bottom: multi-layer spherical geometry used for evaluation of the strain localization coefficients.

seem to have important consequences on model predictions. The relative simplicity of the chosen REV is of great practical importance in what concerns the number of model parameters and the facility and accessibility of their experimental evaluation. The cement matrix mechanical parameters can be measured on a hardened sample of a slurry prepared with the same composition, without HGMS. The HGMS dimensions and mechanical parameters are usually provided by the manufacturer and the information related to the volume fraction of the phases can be easily calculated from the slurry formulation, as presented in the following parts of the paper. In comparison, a more complex REV would need much more detailed information concerning the cement microstructure phase composition, volume fraction and mechanical properties of different phases that are more difficult to evaluate [29,30].

It has been shown in our previous work [21] that there is an excellent interaction between HGMS and cement matrix. HGMS are acting as nucleation agents which implies that cement hydration products are forming on their surface. Furthermore, HGMS present pozzolanic activity, which make them react with the calcium hydroxide formed during cement hydration to form further calcium silicate hydrate. For these reasons, considering a perfect interface between the HGMS and cement matrix does not seem to be a strong assumption for the precision needed for most practical applications. This being said, the effect of imperfect interfaces between HGMS and cement matrix will also be presented and briefly studied in the paper.

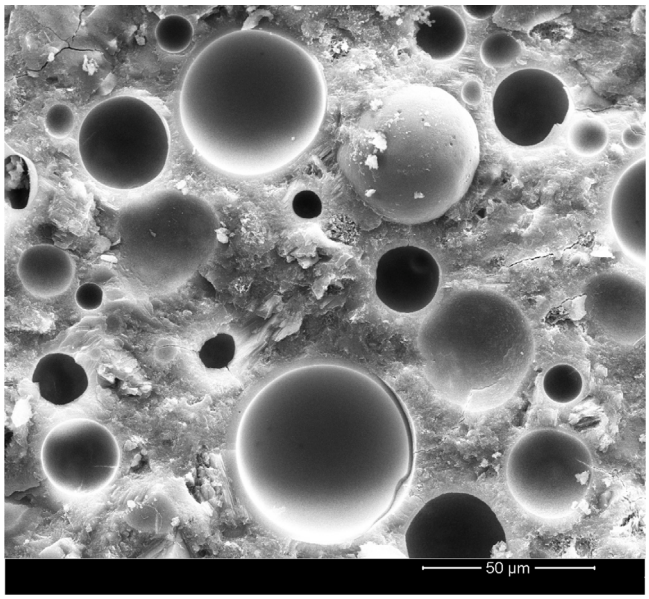

Fig. 5. SEM image of HGMS cement paste after 100 days of curing.

Another point that should be mentioned in relation to the pozzolanic activity of HGMS [21] is that it will consume the glass outer shell to some extent. This will provide amorphous silica that will react with the portlandite present in the cement paste to form calcium silicate hydrate. This process will decrease the thickness of the spheres and affect the chemical composition, microstructure and, eventually, the mechanical parameters of the cement matrix in the vicinity of the HGMS. It should be noted that, in general terms, the degree of pozzolanic reaction is not 100% but rather less than 50% for most cases [31,32]. This results in the pozzolanic additions not being completely consumed by this reaction, a matter that can be verified in Fig. 5, where the existence of HGMS in the cement pastes tested in this work can still be appreciated. To adequately take into account the influence of pozzolanic reactions in the micromechanical model it is necessary to obtain precise information on the zone influenced by the pozzolanic reactions, including the kinetics of the reaction and its effect on the HGMS thickness, the area of the influence zone in the cement matrix and resulted changes in mechanical properties. The mechanical properties of the influence zone may be evaluated by experimental methods like nanoindentation. It is then possible to adapt the REV to take into account the modifications resulted from pozzolanic reactions in the model. This is however out of the scope of this paper and both the HGMS and the cement matrix are assumed to keep their initial dimensions.

The evaluation of the homogenized elastic parameters from Eq. (1) needs the knowledge of the volume fraction of different microstructure phases of the REV. The volume fraction of HGMS in the slurry, f_{HGMS}, can be evaluated by knowing the HGMS mass per unit volume of the slurry and the HGMS density. The necessary volume fraction of the three microstructure phases of the REV (void, glass and cement matrix), can then be evaluated by knowing the HGMS internal and external radii.

$$f_1 = \left(\frac{r_1}{r_2}\right)^3 f_{\mathrm{HGMS}} \quad ; \quad f_2 = \left[1 - \left(\frac{r_1}{r_2}\right)^3\right] f_{\mathrm{HGMS}} \quad ;$$
$$f_3 = 1 - f_1 - f_2 = 1 - f_{\mathrm{HGMS}} \tag{2}$$

The density of the lightweight cement can be evaluated as:

$$\frac{\rho}{\rho_3} = 1 - f_{\mathrm{HGMS}} \left[1 - \frac{\rho_2}{\rho_3}\left(1 - \left(\frac{r_1}{r_2}\right)^3\right)\right] \tag{3}$$

where ρ_2 and ρ_3 are respectively the glass and cement matrix densities.

3.2. Strain localization coefficients

Due to the particular geometry of the inclusions, i.e. hollow spheres, the strain localization coefficients can no more be evaluated based on the classical Eshelby's solution [27]. Instead, the multi-layer spheres solution developed by Hervé and Zaoui [19] is adapted based on the three layer geometry shown in the bottom part of Fig. 4. This solution is based on the assumption of the linear elastic behavior of the cement matrix and the glass material, as well as the existence of a perfect contact between the HGMS and the cement matrix. The presence of an imperfect interface between the cement matrix and HGMS inclusions will be taken into account based on an extension of Hervé and Zaoui [19] model by Ghabezloo [20].

A detailed mathematical development of the strain localization coefficients is given in the appendix of the paper. The essential final equations for a numerical application of the model are presented below, in a way that the strain localization coefficients can be calculated without referring to the appendix. The presentation is done first by assuming perfect interfaces between HGMS and cement matrix. An extension is then presented to take into account the influence of imperfect interfaces.

3.2.1. Perfect interface between HGMS and cement matrix

The coefficients A_k^v and A_k^d to be used in Eq. (1) are given by the following expressions:

$$A_k^v = \frac{H_k^v}{\sum_{k=1}^n f_k H_k^v} \quad ; \quad A_k^d = \frac{H_k^d}{\sum_{k=1}^n f_k H_k^d} \tag{4}$$

The coefficients H_k^v and H_k^d can be evaluated by knowing the geometrical properties of the REV, mainly the radii r_1 and r_2 (cf. Fig. 4), and the elastic properties of glass and cement matrix, respectively referred to by superscripts 2 and 3 (e.g. k_2 is the bulk modulus of glass and g_3 is the shear modulus of the matrix). The coefficients H_k^v are given by the following expressions:

$$H_1^v = \frac{\left(4g_2 + 3k_2\right)\left(4g_3 + 3k_3\right)}{12\left(\frac{r_1}{r_2}\right)^3 k_2\left(g_3 - g_2\right) + 4g_2\left(4g_3 + 3k_2\right)} \tag{5}$$

$$H_2^v = \frac{4g_2}{\left(4g_2 + 3k_2\right)} H_1^v \tag{6}$$

$$H_3^v = 1 \tag{7}$$

It is interesting to note that the H_k^v parameters, and consequently the homogenized bulk modulus evaluated from Eq. (1), depend only on the ratio r_2/r_1 of the HGMS and are independent of the actual values of r_1 and r_2. For obtaining the expressions of H_k^d, it is necessary to calculate the $\mathbf{P}^{(2)}$ matrix, which is a 4 × 4 matrix given by:

$$\mathbf{P}^{(2)} = \mathbf{L}_3^{-1}\left(r_2\right)\mathbf{L}_2\left(r_2\right)\mathbf{L}_2^{-1}\left(r_1\right)\mathbf{L}_1\left(r_1\right) \tag{8}$$

where the matrices $\mathbf{L}_k(r)$ are given by:

$$\mathbf{L}_k(r) = \begin{bmatrix} r & -\frac{6\nu_k}{1-2\nu_k}r^3 & \frac{3}{r^4} & \frac{5-4\nu_k}{1-2\nu_k}\frac{1}{r^2} \\ r & -\frac{7-4\nu_k}{1-2\nu_k}r^3 & -\frac{2}{r^4} & \frac{2}{r^2} \\ g_k & \frac{3\nu_k}{1-2\nu_k}g_k r^2 & -\frac{12}{r^5}g_k & \frac{2(\nu_k-5)}{1-2\nu_k}\frac{g_k}{r^3} \\ g_k & -\frac{7+2\nu_k}{1-2\nu_k}g_k r^2 & \frac{8}{r^5}g_k & \frac{2(1+\nu_k)}{1-2\nu_k}\frac{g_k}{r^3} \end{bmatrix} \tag{9}$$

Note that the superscript (2) in $\mathbf{P}^{(2)}$ is not a power. In accordance with the notations of Hervé and Zaoui [19] it is used to attribute the matrix to the phase 2. The mathematical expressions obtained by calculating each of the components of the $\mathbf{P}^{(2)}$ matrix are considerably long. Since they can be obtained from a multiplication of matrices, the equations of the H_k^d expressed in terms of the components of matrix $\mathbf{P}^{(2)}$, $P_{11}^{(2)}$, $P_{12}^{(2)}$, $P_{21}^{(2)}$, $P_{22}^{(2)}$, as presented below. It should be noted that these components do not all have the same physical unit. $P_{11}^{(2)}$ and $P_{22}^{(2)}$ have no unit, while $P_{12}^{(2)}$ has unit L^2 and $P_{21}^{(2)}$ has unit L^{-2}.

$$H_1^d = \frac{21P_{21}^{(2)}r_1^2 + 5P_{22}^{(2)}}{5\left(P_{11}^{(2)}P_{22}^{(2)} - P_{12}^{(2)}P_{21}^{(2)}\right)} \tag{10}$$

$$H_2^d = \frac{P_{21}^{(2)}}{5\left(\nu_2 - 1\right)\left(P_{11}^{(2)}P_{22}^{(2)} - P_{12}^{(2)}P_{21}^{(2)}\right)} \left[\frac{P_{22}^{(2)}\left(5\nu_2 - 7\right)}{3P_{21}^{(2)}} + 7r_1^2\left(\nu_2 - 1\right) - \frac{84\left(r_1^5 - r_2^5\right)}{5\left(r_1^3 - r_2^3\right)}\right] \tag{11}$$

$$H_3^d = 1 \tag{12}$$

In the above equations r_1 and r_2 are respectively the internal and external radii of HGMS. k_k, g_k and ν_k stand respectively for bulk modulus, shear modulus and Poisson's ratio of the k phase (with void space, silicate glass and cement matrix indexed from 1 to 3, respectively). Note that the elastic parameters of the phase 1 (void space) should be considered equal to zero.

Considering the complexity of the equations of H_k^d parameters, one can numerically verify that, similarly to what was mentioned above for H_k^v parameters, these coefficients and consequently the homogenized shear modulus evaluated using Eq. (1) are independent of the numerical values of r_1 and r_2 and depend only on the ratio r_2/r_1. It can also be verified that by considering similar elastic parameters for phases 2 and 3, the above equations are reduced to the ones given by classical Eshelby solution for a simple porous medium.

It should be noted that considering the phase number 3 as the cement matrix corresponds to the Mori–Tanaka homogenization scheme. A different choice could be the self-consistent scheme in which the reference medium is the homogenized medium. In this latter case, the elastic parameters of the matrix are not known in advance. Consequently, iterative calculations should be used to evaluate the homogenized elastic parameters. Considering the microstructure of the HGMS lightweight cement, Mori–Tanaka scheme seems to be more appropriate. However, comparison tests were performed between the two methods for a variety of parameters. For usual volume fractions of HGMS, the results of these two methods are extremely close together. Therefore, in the following, Mori–Tanaka scheme is used for the calculations since it has the advantage of being easier to apply, in accordance with the main objective of obtaining an easy to apply model for estimating the elastic properties of lightweight cement pastes based on HGMS.

3.2.2. Imperfect interface between HGMS and cement matrix

The above mathematical framework can be extended to take into account the presence of an imperfect interface between the microspheres and the cement matrix. The imperfect interface, characterized by its compliances, results in displacement jumps across the interface. The micromechanical models with imperfect interface has been previously developed and used in the literature [e.g.33–37]. Ghabezloo [20] presented an extension of the micromechanical model of Hervé and Zaoui [19] to take into account imperfect interfaces between phases. This model is used in the following.

The displacement jump at the interface is assumed to be proportional to the traction vector $\sigma_{ij}n_j$ which is continuous across the interface. The following general equation is postulated for the displacement jump across the interface [34,38,39]:

$$\Delta u_i = \eta_{ij}\sigma_{jk}n_k \tag{13}$$

where η_{ij} is a second-order tensor representing the compliances of the interface. $\eta_{ij} = 0$ corresponds to a perfectly bounded interface. A simple

form of η_{ij} with one tangential and one normal compliance, η^t and η^n respectively, can be given as [34,38,39]:

$$\eta_{ij} = \eta^t \delta_{ij} + \left(\eta^n - \eta^t\right) n_i n_j \tag{14}$$

In the presence of imperfect interfaces, the strain localization coefficients of each phase A_k^v and A_k^d can be written as [20]:

$$A_k^v = \frac{H_k^v}{\sum_{k=1}^n f_k \left(1 + 3\lambda_k\right) H_k^v} \tag{15}$$

$$A_k^d = \frac{H_k^d}{\sum_{k=1}^n f_k \left(1 + 2\xi_k \frac{2\psi_k + 3}{5}\right) H_k^d} \tag{16}$$

The following dimensionless parameters have been introduced to simplify the presentation of the equations:

$$\lambda_k = \frac{k_k \eta_k^n}{r_k}; \quad \xi_k = \frac{g_k \eta_k^t}{r_k}; \quad \psi_k = \frac{\eta_k^n}{\eta_k^t} \tag{17}$$

The coefficient H_1^v is given by the following expression:

$$H_1^v = \frac{\left(4g_2 + 3k_2\right)\left(4g_3 + 3k_3\right)}{12\left(\frac{r_1}{r_2}\right)^3 k_2 \left[g_3\left(1 - 4\xi_2\psi_2\right) - g_2\right] + 4g_2\left[4g_3\left(1 + 3\lambda_2\right) + 3k_2\right]} \tag{18}$$

The coefficient H_2^v can be evaluated as a function of H_1^v using Eq. (6) and $H_3^v = 1$, same as Eq. (7). One can easily verify that for a perfect bounding between the HGMS and cement matrix, i.e. $\lambda_2 = \xi_2 = 0$, Eq. (18) is reduced to Eq. (5). To evaluate H^d coefficients the matrix $\mathbf{P}^{(2)}$ can be evaluated as follows:

$$\mathbf{P}^{(2)} = \mathbf{L}_3^{-1}\left(r_2\right)\left[\mathbf{L}_2\left(r_2\right) + \mathbf{L}_2'\left(r_2\right)\right]\mathbf{L}_2^{-1}\left(r_1\right)\mathbf{L}_1\left(r_1\right) \tag{19}$$

where the matrix $\mathbf{L}_k'(r)$ is given by:

$$\mathbf{L}_k'(r) = \begin{bmatrix} g_k\eta_k^n & \frac{3\nu_k}{1-2\nu_k} g_k r^2 \eta_k^n & -\frac{12}{r^5} g_k \eta_k^n & \frac{2\left(\nu_k - 5\right)}{1-2\nu_k}\frac{1}{r^3} g_k \eta_k^n \\ g_k\eta_k^t & \frac{7+2\nu_k}{1-2\nu_k} g_k r^2 \eta_k^t & \frac{8}{r^5} g_k \eta_k^t & \frac{2\left(\nu_k + 1\right)}{1-2\nu_k}\frac{1}{r^3} g_k \eta_k^t \\ 0 & 0 & 0 & 0 \\ 0 & 0 & 0 & 0 \end{bmatrix} \tag{20}$$

The matrices $\mathbf{L}_k(r)$ are given by Eq. (9). The coefficients H_1^d, H_2^d and H_3^d are then evaluated using Eqs. (10), (11) and (12) respectively.

4. Sensitivity analysis

To understand the model parameters and their influence on the evaluated elastic parameters, a sensitivity analysis is undertaken. For this purpose, it is useful to recall Eq. (1) showing that the homogenized elastic parameters will depend on the volume fraction of each phase, f_k, the elastic properties of each phase, k_k and g_k, and the localization coefficients, A_k^v and A_k^d, which play the roles of some weighting factors. As shown in Eqs. (5) to (12), these parameters depend on the elastic properties of each phase and on the radii ratio r_2/r_1. It is obvious that using a cement matrix with higher elastic parameters results directly in a cement paste with higher parameters. This is the same for the HGMS material, an increase in its elastic parameters is directly reflected on the elastic parameters of the paste, though with a less important effect as compared to cement paste due to its lower volume fraction.

It is interesting to see the effect of the ratio r_2/r_1 and HGMS volume fraction on the homogenized elastic parameters of the HGMS lightweight cement while keeping constant the other parameters. The Young's modulus and the Poisson's ratio of the silica glass and the cement matrix are given the values of $E_2 = 64$ GPa, $\nu_2 = 0.2$, $E_3 = 22$ GPa and $\nu_3 = 0.25$. The needed values of bulk and shear moduli can be evaluated using $K = E/[3(1-2\nu)]$ and $G = E/[2(1+\nu)]$. A perfect interface is assumed between the cement matrix and HGMS. The results of sensitivity analysis are presented as contour graphs in Fig. 6 for the bulk modulus and in Fig. 7 for the shear modulus for different values of f_{HGMS} and r_2/r_1 ratio. The homogenized elastic parameters are normalized with respect to the elastic parameters of the cement matrix. The normalized cement slurry density corresponding to each case can be evaluated using Eq. (3).

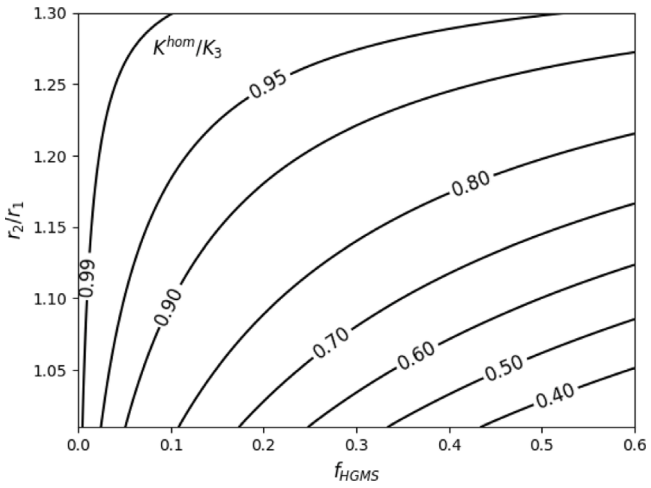

Fig. 6. Effect of HGMS volume fraction and the radii ratio r_2/r_1 of HGMS on the homogenized bulk modulus (perfect interface is assumed between HGMS and cement matrix).

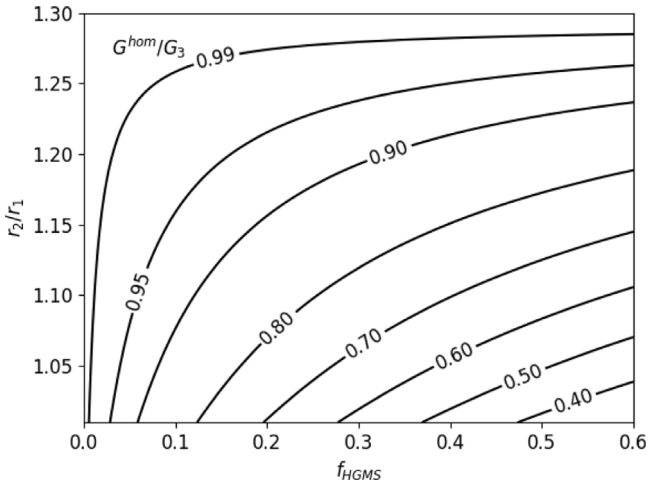

Fig. 7. Effect of HGMS volume fraction and the radii ratio r_2/r_1 of HGMS on the homogenized shear modulus (perfect interface is assumed between HGMS and cement matrix).

One can see in Figs. 6 and 7 that the results are in agreement with expectations. For constant HGMS volume fraction, both bulk and shear moduli increase with increasing r_2/r_1 ratio, which implies increasing the glass (phase 2) to void (phase 1) proportion in the composite medium. If the volume fraction of glass increases and the void volume fraction decreases, greater amounts of stiff material will increase the stiffness of the composite material. Therefore using thicker HGMS results in higher elastic moduli, but also, in higher density of the cement paste, which is less desirable. At constant HGMS dimensions, higher HGMS volume fraction results in a lighter cement paste, but also in lower elastic parameters. Recalling Figs. 1 and 2, it is clear that HGMS's void volume fraction is much larger than the borosilicate glass volume fraction. Increasing the HGMS volume fraction implies increasing the void space, which decreases the homogenized elastic parameters.

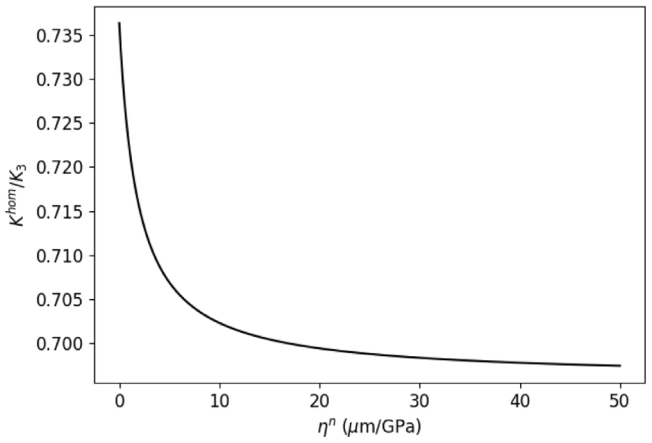

Fig. 8. Effect of interface normal compliance on the homogenized bulk modulus.

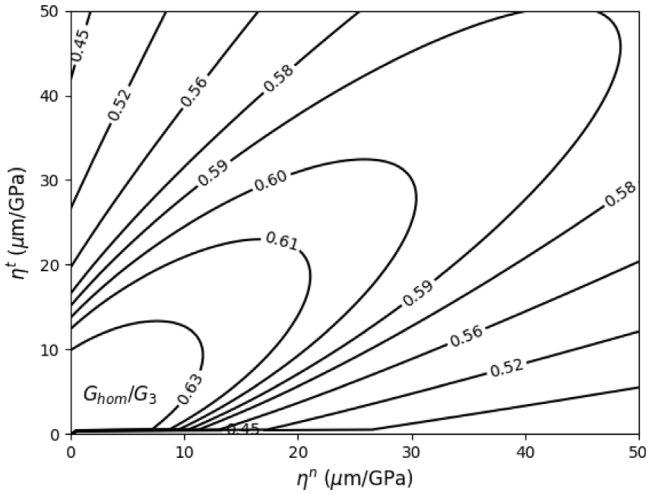

Fig. 9. Effect of interface normal and tangential compliances on the homogenized shear modulus.

It is also interesting to see how the existence of an imperfect interface between the cement matrix and HGMS can influence the evaluated elastic moduli. For this analysis the internal and external radii of the HGMS are fixed respectively equal to $r_1 = 18$ μm and $r_2 = 20$ μm. HGMS volume fraction is taken equal to 0.24. The homogenized bulk and shear moduli are evaluated for a wide range of interface normal and tangential compliances. The homogenized bulk modulus depends only on the normal compliance and is independent of the tangential compliance. Its variations with the normal compliance are plotted in Fig. 8. The evaluated bulk moduli are normalized with respect to the matrix bulk modulus. $\eta^n = 0$ corresponds to a perfect interface. The results show that the bulk modulus decreases by increasing the interface compliance, but tends towards an asymptotic value. Generally, it seems that the presence of an imperfect interface between HGMS and cement matrix has a limited influence on the bulk modulus. For the parameters used in the sensitivity analysis the ratio K^{hom}/K_3 is reduced from 0.736 for the perfect interface to 0.696 for a highly compliant interface.

The influence of interface normal and tangential compliances on the homogenized shear modulus is presented in Fig. 9 in the form of a contour plot. One can see a complex interaction between the effects of normal and tangential compliances on the homogenized shear modulus. An important difference between the two compliances, e.g. big η^n and small η^t or inverse, results in lower shear modulus. In the particular case of $\eta^n = \eta^t$ an asymptotic influence can be observed. For the parameters used in the sensitivity analysis the ratio G^{hom}/G_3 is reduced from 0.76 for the perfect interface to an 0.54 for a highly compliant interface.

5. Application

In this section, the proposed model is applied to some particular formulations of cement pastes with addition of HGMS. A comparison between laboratory and model results is performed.

5.1. Sample preparation

The cement used for this purpose is a class G moderate sulphate-resistant portland cement [40] provided by Petroquímica Comodoro Rivadavia (Argentina), mixed with HGMS27 and HGMS41 from 3M, polycarbonate-based superplasticizer (SP) (ADVA 570, GCP Applied Technologies) and deionized water. HGMS27 and HGMS41 have respectively crush strengths of 27 and 41 MPa, densities of 280 kg/m^3 and 460 kg/m^3, and mean particle size (D50) of 30 μm and 40 μm.

Cement slurries were designed with two water to solids weight ratios (w/s) of 0.44 and 0.60 and HGMS were added as 10% in weight cement replacement. The classifications and dosages of cement slurries are presented in Table 1. CS refers to cement slurry, the two following numbers correspond to HGMS (00: no HGMS, 27: HGMS27, 41: HGMS41) and the two last numbers correspond to the w/s (0.44 and 0.60).

Table 1
Slurries classification, dosages and densities.

Slurry	Cement [kg/m^3]	HGMS27 [kg/m^3]	HGMS41 [kg/m^3]	Water [kg/m^3]	SP [kg/m^3]	ρ [kg/m^3]
CS0044	1320.2	–	–	580.9	–	1988
CS2744	829.0	92.1	–	405.3	2.8	1388
CS4144	952.5	–	105.8	465.6	2.1	1601
CS0060	1313.8	–	–	788.3	–	1803
CS2760	828.3	92.0	–	552.2	–	1287
CS4160	950.6	–	105.6	633.7	–	1472

Cement samples were prepared following the guidelines of the American Petroleum Institute (API) Recommended Practice [41]. For this purpose, a specially designed mixing machine with the capability of reaching the high revolutions per minute required was used. According to the API, water shall be added to the mixing machine followed by the cement, which is added while the mixing machine is working. Then the mixing time is reached and the molds are filled with the cement slurry.

For CS27 and CS41, given the important difference in density between HGMS and cement, these materials needed to be mixed before. Therefore, the necessary amount of each of them was poured into a vessel and mixed by hand until reaching a homogeneous dry material. Due to the decrease in fluidity that HGMS generate for cement slurries CS2744 and CS4144 it was necessary to add some superplasticizer. With this additive it was feasible to reach an homogeneous wet mixture by applying the specified mixing energy [21].

For evaluation of the mechanical parameters, for each formulation six cylindrical molds were filled with the cement slurry. The molds have a diameter of 3.8 centimeters and a height of 10 centimeters. The samples were immersed in water saturated with lime for 28 days and subsequently stored in isolation until they reached the age of 100 days. The cement hydration is expected to have reached the asymptotic stage at this age. The samples were then cut using a diamond wire saw to obtain specimens with a height-to-diameter ratio of 2, remove the exposed faces formed during the initial curing process, and achieve flat and parallel faces.

5.2. Experimental evaluation of elastic parameters

Ultrasonic wave velocity measurements were conducted on the six samples of each paste to obtain their elastic parameters, which

Table 2
Measured ultrasonic wave velocities.

Paste	V_p		V_s	
	Mean [m/s]	SD [m/s]	Mean [m/s]	SD [m/s]
CS0044	3800	41.80	2210	70.34
CS2744	3340	32.56	1980	11.88
CS4144	3580	15.20	2070	22.68
CS0060	3370	28.04	1880	22.17
CS2760	3090	15.05	1760	7.86
CS4160	3270	25.65	1840	6.73

Table 3
Elastic properties (determined from ultrasonic wave velocities).

Slurry	E [GPa]	K [GPa]	G [GPa]	ν [–]
CS0044	24.1	15.7	9.7	0.24
CS2744	13.4	8.3	5.4	0.23
CS4144	17.1	11.4	6.8	0.25
CS0060	16.3	12.0	6.4	0.27
CS2760	10.1	6.9	4.0	0.26
CS4160	12.7	9.1	5.0	0.27

are expected to be comparable to those from quasi-static mechanical tests, with some possible differences arising from factors such as poromechanical effects or creep [28,42,43].

The measured wave velocities are shown in Table 2, with mean values and standard deviation (SD) for each slurry. From these results, the elastic parameters of each slurry were deduced according to Eq. (21). The needed densities are given in Table 1. These were obtained by measuring the mass and the volume of each saturated cement sample. To determine the mass densities, the mass of each sample was measured using a calibrated analytical balance with a resolution of 0.001 g. The volume of each sample was measured using a calibrated Vernier caliper with a resolution of 0.01 mm, measuring the diameter at three different heights and taking the average. The height was also measured three times, with the sample rotated slightly each time to ensure that the measurements were representative of the entire sample.

All measurements were conducted under controlled laboratory conditions to minimize environmental influences on the data. Using these precise instruments and procedures, we obtained mass density results with a standard deviation of 20 kg/m^3 or less.

$$G = \rho V_s^2 \quad ; \quad K = \rho\left(V_p^2 - \frac{4}{3}V_s^2\right) \tag{21}$$

Eq. (21) for calculating K and G is valid for homogeneous, isotropic and linear elastic materials, but they could be applied to heterogeneous materials as long as the size of the representative elementary volume (d) is much smaller than the wavelength of the ultrasonic pulse used (λ) [44]. This is known as the separation of scale requirement, and it should be verified since lightweight cement pastes used in this research are heterogeneous materials. For the measurements in this study, the frequency of the ultrasonic pulse was 500 kHz. With the measured velocities, presented in Table 3, the evaluated wavelength is at least 3.5 mm, which is significantly larger than the microspheres and the REV of the material (see Fig. 5) to consider that the separation of scale requirement is satisfied ($d \ll \lambda$).

By evaluation of the bulk and shear moduli, the other elastic parameters (E and ν) can then be evaluated using classical relationships between elastic parameters. The measured values of elastic parameters are shown in Table 3. It can be seen that, as expected, higher w/s ratio (CS0044 vs. CS0060, CS2744 vs. CS2760 and CS4144 vs. CS4160) results in pastes with lower elastic moduli. Furthermore, pastes with HGMS (CS2744, CS4144, CS2760, CS4160) have lower moduli as compared to plain cement pastes (CS0044, CS0060) with the same w/s ratio.

Table 4
Model parameters for different cement pastes.

Parameter	CS2744	CS4144	CS2760	CS4160
r_1 (μm)	14.344	18.518	14.344	18.518
r_2 (μm)	15.000	20.000	15.000	20.000
f_{HGMS}	0.329	0.230	0.287	0.197
f_1	0.288	0.183	0.251	0.156
f_2	0.041	0.047	0.036	0.041
f_3	0.671	0.770	0.713	0.803
E_2 (GPa)	64.0	64.0	64.0	64.0
E_3 (GPa)	24.1	24.1	16.3	16.3
ν_2	0.20	0.20	0.20	0.20
ν_3	0.24	0.24	0.27	0.27

5.3. Model predictions considering perfect interface

For applying this homogenization model to cement pastes with HGMS, it was considered that the matrix of these pastes was composed of cement paste with the same elastic properties as those of CS0044 and CS0060 for each w/s ratio, respectively. In addition, Table 4 shows all the necessary parameters for different cement pastes. The HGMS volume fractions are evaluated from the slurries composition, specified in Table 1 and the density of each component. The volume fractions of phases are then evaluated using Eq. (2). The outer radius r_2 is given as the D_{50} of the HGMS, while the inner radius r_1 is determined by knowing the density of the HGMS ($\rho_{\text{HGMS27}} = 0.28$ g/cm^3, $\rho_{\text{HGMS41}} = 0.46$ g/cm^3) and the borosilicate glass ($\rho_2 = 2.23$ g/cm^3) using the following equation:

$$r_1 = r_2\left[1 - \frac{\rho_{\text{HGMS}}}{\rho_2}\right]^{1/3} \tag{22}$$

Finally, the properties of the borosilicate glass forming the outer shell are obtained from the literature [45,46]. It should be emphasized that no parameter calibration or fitting is done.

A perfect interface is first assumed between the HGMS and the cement matrix. Figs. 10 and 11 present comparisons between the evaluated and experimentally measured bulk and shear moduli for different cement pastes. It can be appreciated that the model predictions assuming the perfect interface, needless of any calibration, are in quite good agreement with those of laboratory tests, with differences lower than 15%. The biggest difference between the model prediction and experimental results is related to cement paste CS2760, which is the lightest paste among all that were studied given the higher w/s ratio and the lower specific weight of HGMS27 as compared to HGMS41. It is interesting to notice that the model predictions for all the studied pastes are slightly higher than the laboratory results.

5.4. Effect of interface between HGMS and cement matrix

The difference between the model predictions and the experimental results, which is less than 15% for the studied samples, is probably negligible for most practical applications. This can be due to simultaneous effects of various factors and simplifications assumptions related to the homogenization method, the configuration of the REV, and the perfect interface between HGMS and cement matrix. Considering the overestimation of the elastic parameters compared to the measured values, as can be seen in Figs. 10 and 11, it is interesting to see if the model predictions can be improved by considering an imperfect interface between the HGMS and the cement matrix. The interface parameters can be fitted to minimize the error between the model predictions and experimental results. The studied samples have different w/s ratios and different HGMS dimensions. Consequently, the interfaces in these samples are not necessarily similar. However, for the sake of simplicity, it is assumed that the interfaces in all samples have the same normal and tangential compliances.

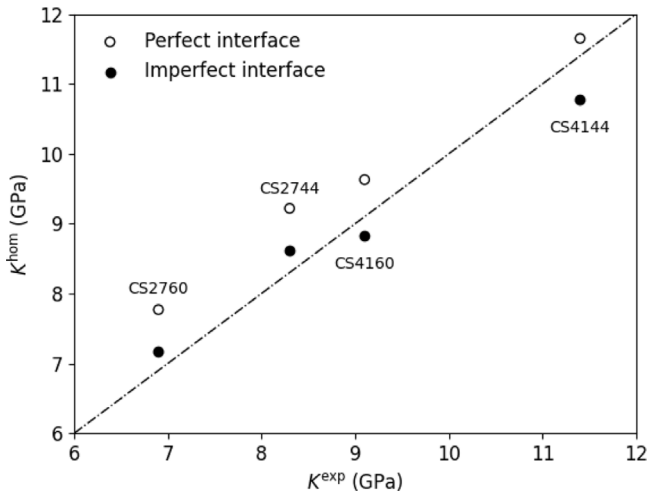

Fig. 10. Comparison between experimentally evaluated bulk moduli of different samples and model predictions considering perfect and imperfect interfaces.

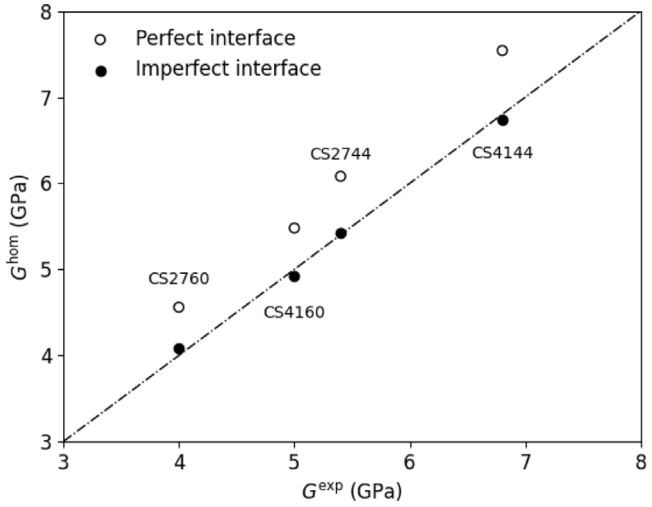

Fig. 11. Comparison between experimentally evaluated shear moduli of different samples and model predictions considering perfect and imperfect interfaces.

The fitting of interface parameters is done by evaluating the error, defined in Eq. (23), between the model predictions and experimental results by varying the interface parameters, η^n and η^t, in a large span.

$$\text{Error} = \sum_{i=1}^{4}\left[\left(\frac{K_i^{\text{hom}} - K_i^{\text{exp}}}{K_i^{\text{exp}}}\right)^2 + \left(\frac{G_i^{\text{hom}} - G_i^{\text{exp}}}{G_i^{\text{exp}}}\right)^2\right] \tag{23}$$

The results are presented in the contour plot of Fig. 12. The minimum error is found equal to 7.66×10^{-3} for the interface parameters $\eta^n = 1.215$ μm/GPa and $\eta^t = 2.527$ μm/GPa. The fact that for the fitted values $\eta^n < \eta^t$ is compatible with the available information in the literature [38,47,48]. It is interesting to mention that the evaluated error for the case of perfect interfaces is 115×10^{-3}.

The model predictions for the fitted interface parameters are presented in Figs. 10 and 11. Obviously the predictions are much closer to the experimental values, with very small differences in bulk modulus and almost perfect predictions for shear modulus.

6. Conclusion

An analytical model, based on the homogenization theory, is proposed to predict the elastic properties of light-weight cement pastes prepared with hollow glass microspheres. The model is simple and needs the knowledge of the elastic properties of the cement matrix, as well as the volume fraction of HGMS, their dimensions and elastic properties. The existence of an imperfect interface between the microspheres and the cement matrix can also be taken into account in the model. A sensitivity analysis showed that the model results depend particularly on the changes in the ratio of external to internal radii of microspheres and also to cement matrix properties. The existence of an imperfect interface between the microspheres and the cement matrix has a limited effect on the predicted bulk modulus, but depending on the interface parameters, can have a more important effect on the predicted shear modulus. The model predictions have been compared to experimental data, showing a very good comparison. Without any parameter calibration for the case of perfect interface, the model predictions, with less than 15% difference with experimental values, are adequate for most practical applications. The fitting of a single pair of interface parameters, normal and tangential compliances, for all tested slurries, permitted to significantly improve the model predictions. This model is a useful tool for engineers in the design of lightweight cement slurry formulations based on hollow glass microspheres.

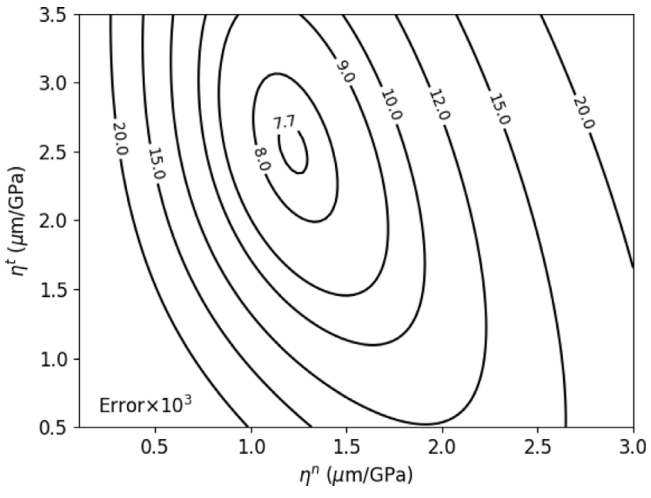

Fig. 12. Fitting of the interface parameters. Contour plot of error for different values of normal and tangential compliances.

CRediT authorship contribution statement

Christian Marcelo Martín: Software, Validation, Formal analysis, Writing – original draft, Visualization, Investigation. **Siavash Ghabezloo:** Conceptualization, Methodology, Resource, Data curation, Writing – review & editing, Supervision. **Teresa María Piqué:** Validation, Visualization, Investigation, Writing – review & editing. **Jean-Michel Pereira:** Validation, Supervision, Funding acquisition, Writing – review & editing. **Diego Guillermo Manzanal:** Validation, Supervision, Project administration, Funding acquisition, Writing – review & editing.

Declaration of competing interest

The authors declare the following financial interests/personal relationships which may be considered as potential competing interests: Diego Manzanal reports financial support was provided by European Commission.

Data availability

Data will be made available on request.

Acknowledgments

The first author gratefully acknowledges the EIFFEL fellowship program of Excellence granted by the Ministère de l'Europe et des Affaires étrangères of France. The authors acknowledged the financial support of the European Union's Horizon 2020 research and innovation program under Grant Agreement No 101007851 (H2020 MSCA-RISE 2020 Project DISCO2-STORE), the Agency of Scientific and Technological Promotion from the Argentine Republic. (PICT 2020-SERIEA 02088), UNPSJB PI1614 80020190200006 IP, Res. R/9N° 207–2020 CRD1365 FI004/ 17, UBACYT 20020190200005BA and the PIP project N° 11220200103043CO (CONICET). The authors also thank the technical staff of Laboratoire Navier for their contribution in the experimental program.

Appendix. Theoretical framework of the model

This appendix is dedicated to the presentation of the theoretical framework of the model. The final equations are presented in the main text, in a way that the model can be used without referring to the appendix. It should be emphasized that no originality is claimed concerning the equations presented in this appendix, most of the content can be found in Hervé and Zaoui [19] and Ghabezloo [20]. However we think that a unified presentation of this framework permits the paper to be almost standalone and easier to read and to understand. The model framework is presented for a general case including the effect of imperfect interface between phases. It can be reduced to the case with perfect interfaces by setting the interface compliances equal to zero.

A.1. Homogenization method

The aim of classical homogenization method is to replace an actual heterogeneous complex body by a fictitious homogeneous one that behaves globally in the same way. The theoretical framework of micromechanics modeling and homogenization method has been presented in different papers and textbooks, e.g. [10,11]. The principles and main equations of this framework are presented briefly in the following.

The volume V_0 of the REV (Representative Elementary Volume) of a heterogeneous material is composed of n different phases with volumes V_k, $r = 1 \ldots n$, and volume fractions $f_k = V_k/V_0$. The tensors of elastic moduli of each phase is denoted by $\mathbf{c}_k$. In the case of isotropy of the solid phases, the tensor of elastic moduli can be written as the sum of a volumetric and a deviatoric part, $\mathbf{C}_k = 3k_k\mathbf{J} + 2g_k\mathbf{K}$, where k_k and g_k are the bulk modulus and shear modulus of the phase k respectively. $\mathbf{J}_{pqrs} = \frac{1}{3}\delta_{pq}\delta_{rs}$ is the volumetric part of the fourth-order symmetric unit tensor $\mathbf{I}$ and $\mathbf{K} = \mathbf{I} - \mathbf{J}$ is the deviatoric part. $\mathbf{I}$ is defined as $\mathbf{I}_{pqrs} = \frac{1}{2}\left(\delta_{pr}\delta_{qs} + \delta_{ps}\delta_{qr}\right)$ and δ_{pq} stands for the Kronecker delta. The homogenization equations for the effective elastic properties can be derived on a REV submitted to a homogeneous strain boundary conditions. The homogeneous strain boundary conditions are associated to prescribed displacements $\underline{u}$ at the boundary of the REV as $\underline{u} = \mathbf{E} : \underline{x}$, where $\underline{x}$ is the microscopic position vector and $\mathbf{E}$ is the macroscopic strain tensor. It can be shown that $\mathbf{E}$ is equal to the volume average of the microscopic compatible (i.e., derived from a displacement field) strain field $\boldsymbol{\varepsilon}(\underline{x})$ in the REV [11], $\mathbf{E} = \langle\boldsymbol{\varepsilon}\rangle_V$ where $\langle z\rangle_V = (1/V)\int_V z(\underline{x})\,dV$ stands for the volume average of quantity z over domain V.

In the framework of linear elasticity, the local strain field $\boldsymbol{\varepsilon}(\underline{x})$ is related to macroscopic strain $\mathbf{E}$ through fourth-order localization tensor $\mathbf{A}(\underline{x})$:

$$\boldsymbol{\varepsilon}(\underline{x}) = \mathbf{A}(\underline{x}) : \mathbf{E} \tag{A.1}$$

Using the equality $\mathbf{E} = \langle\boldsymbol{\varepsilon}\rangle$, one obtains $\langle\mathbf{A}\rangle = \mathbf{I}$. The tensor of overall effective moduli $\mathbf{C}^{\text{hom}}$ of the heterogeneous porous material is given as:

$$\mathbf{C}^{\text{hom}} = \langle\mathbf{c} : \mathbf{A}\rangle \tag{A.2}$$

The above equation is classical and has been presented in many different papers [e.g.10,11]. In the isotropic case, this equation is reduced to the following forms:

$$K^{\text{hom}} = \sum_{k=1}^{m} f_k k_k A_k^v \quad ; \quad G^{\text{hom}} = \sum_{k=1}^{m} f_k g_k A_k^d \tag{A.3}$$

The evaluation of the effective elastic moduli needs an estimations of the strain localization tensor $\mathbf{A}$. This needs the knowledge of the stress and strain fields in an inclusion embedded in an infinite medium and subjected to homogeneous strain $\mathbf{E}_0$ at infinity. The general form of the solution can be considered as follows:

$$\varepsilon^{(k)} = \mathbf{H}_k : \mathbf{E}_0 \tag{A.4}$$

where the tensor $\mathbf{H}_k$ is a function of the elastic moduli of the inhomogeneity and the reference medium, $\mathbf{C}_k$ and $\mathbf{C}_0$, respectively and the geometry of the inclusion. Eshelby [27] gives the solution for the stress and strain fields inside an ellipsoidal inhomogeneity perfectly bounded to an infinite elastic reference medium.

As explained by Zaoui [11], the strain localization tensor can be estimated by estimating the average mechanical state in each phase k of the RVE subjected to the macroscopic strain $\mathbf{E}$ as that of an ellipsoidal inhomogeneity with the same moduli, embedded in an infinite matrix with arbitrary moduli C_0 subjected to some adequate uniform strain at infinity $\mathbf{E}_0$. The stress and strain field in the phase k are thus estimated by Eq. (A.4). The strain tensor $\mathbf{E}_0$ can be determined knowing that $\mathbf{E} = \langle\varepsilon\rangle$:

$$\mathbf{E} = \langle\varepsilon\rangle = \langle\mathbf{H}\rangle : \mathbf{E}_0 \tag{A.5}$$

Inserting $\mathbf{E}_0$ from this relation in Eq. (A.4) and comparing with Eq. (A.1), the strain localization tensor of the phase k can be identified:

$$\mathbf{A}_k = \mathbf{H}_k : \langle\mathbf{H}\rangle^{-1} \tag{A.6}$$

A.1.1. Average strain in a REV with imperfect interfaces

This approach could be extended by considering the existence of an imperfect interface between a phase and its surrounding medium. The presence of imperfect interface results in a displacement jump given by $\Delta u_i = \eta_{ij}\sigma_{jk}n_k$, where η_{ij} is interface compliance tensor. η_{ij} can be expressed in terms of η^n and η^t, which are respectively normal and tangential compliances. [20,34,39].

$$\eta_{ij} = \eta^t\delta_{ij} + \left(\eta^n - \eta^t\right)n_i n_j \tag{A.7}$$

The average strain over the REV considering displacement jumps at the interfaces is given by:

$$\langle\boldsymbol{\varepsilon}\rangle_V = \frac{1}{V}\int_V \boldsymbol{\varepsilon}(\underline{x})\,dV = \sum_{k=1}^{m} f_k\boldsymbol{\varepsilon}_k + \frac{1}{2V}\sum_{k=1}^{m}\int_s \left(\Delta u_i n_j + \Delta u_j n_i\right)ds \tag{A.8}$$

The strain tensor $\mathbf{E}_0$ can be determined knowing that $\mathbf{E} = \langle\boldsymbol{\varepsilon}\rangle$, by inserting Eq. (A.4) in Eq. (A.8):

$$\mathbf{E} = \langle\boldsymbol{\varepsilon}\rangle_V = \sum_{r=1}^{n} f_k\mathbf{H}_k : \mathbf{E}_0 + \frac{1}{2V}\sum_{k=1}^{m}\int_s \left(\Delta u_i n_j + \Delta u_j n_i\right)ds \tag{A.9}$$

The term Δu in Eq. (A.9) can be replaced with the expression of the displacement jump to find:

$$\mathbf{E} = \sum_{k=1}^{m} f_k\mathbf{H}_k : \mathbf{E}_0 + \frac{1}{2V}\sum_{k=1}^{m}\int_s \left(\eta_{im}\sigma_{mk}n_k n_j + \eta_{jm}\sigma_{mk}n_k n_i\right)ds \tag{A.10}$$

Considering the difficulty of the evaluation of the integral term in the above equation, an *ad hoc* approximation can be formulated by replacing the stress on the interface by its average over the inclusion [20, 34,37,39].

$$\int_s \left(\eta_{im}\sigma_{mk}n_k n_j + \eta_{jm}\sigma_{mk}n_k n_i\right)ds \simeq \bar{\sigma}_{mk}\int_s \left(\eta_{im}n_k n_j + \eta_{jm}n_k n_i\right)ds \tag{A.11}$$

The calculation of the integral in Eq. (A.11) needs the evaluation of the integral $\int_s \eta_{ij} n_k n_l ds$. Using Eq. (A.7) this can be written as:

$$\int_s \eta_{ij} n_k n_l ds = \int_s \left[\eta^t \delta_{ij} + \left(\eta^n - \eta^t\right) n_i n_j\right] n_k n_l ds \tag{A.12}$$

The above integral can be calculated using the following two integrals evaluated over a spherical inclusion:

$$\frac{1}{s}\int_s n_i n_j ds = \frac{1}{3}\delta_{ij}; \quad \frac{1}{s}\int_s n_i n_j n_k n_l ds = \frac{1}{15}\left(\delta_{ij}\delta_{kl} + \delta_{ik}\delta_{jl} + \delta_{il}\delta_{jk}\right) \tag{A.13}$$

Using Eqs. (A.12) and (A.13), the integral term in Eq. (A.11) can be written as:

$$\int_s \left(\eta_{im} n_k n_j + \eta_{jm} n_k n_i\right) ds = \frac{s}{15}\left[\left(2\eta^n + 3\eta^t\right)\left(\delta_{im}\delta_{jk} + \delta_{ik}\delta_{mj}\right) + 2\left(\eta^n - \eta^t\right)\delta_{ij}\delta_{mk}\right] \tag{A.14}$$

Knowing that $\mathbf{I}_{ijmk} = \frac{1}{2}\left(\delta_{im}\delta_{jk} + \delta_{ik}\delta_{jm}\right)$ and $\mathbf{J}_{ijmk} = \frac{1}{3}\delta_{ij}\delta_{mk}$, the above equation can be re-written as:

$$\int_s \left(\eta_{im} n_k n_j + \eta_{jm} n_k n_i\right) ds = s\left[\frac{2\eta^n}{3}\mathbf{J} + \frac{4\eta^n + 6\eta^t}{15}\mathbf{K}\right] \tag{A.15}$$

Using Eqs. (A.11) and (A.15), $s = 4\pi r^2$, $V = \frac{4}{3}\pi r^3$ for a spherical inclusion of radius r and $1/V = f_k/V_k$, Eq. (A.10) can be re-written as:

$$\mathbf{E} = \sum_{k=1}^{m} f_k \left(\mathbf{H}_k : \mathbf{E_0} + \boldsymbol{\sigma}^{(k)} : \mathbf{P}^{(k)}\right) \tag{A.16}$$

where

$$\mathbf{P}^{(k)} = \frac{1}{r}\left[\eta_k^n \mathbf{J} + \frac{4\eta_k^n + 3\eta_k^t}{5}\mathbf{K}\right] \tag{A.17}$$

By knowing that $\boldsymbol{\sigma}^{(k)} = \mathbf{C}_k : \boldsymbol{\varepsilon}^{(k)}$ and $\boldsymbol{\varepsilon}^{(k)} = \mathbf{H}^{(k)} : \mathbf{E}_0$ the following can be obtained:

$$\mathbf{E} = \sum_{k=1}^{m} f_k \left(\mathbf{I} + \mathbf{C}_k : \mathbf{P}^{(k)}\right) : \mathbf{H}_k : \mathbf{E_0} = \left\langle \left(\mathbf{I} + \mathbf{C}_k : \mathbf{P}^{(k)}\right) : \mathbf{H}_k \right\rangle : \mathbf{E_0} \tag{A.18}$$

Inserting $\mathbf{E_0}$ from this equation into the $\boldsymbol{\varepsilon}^{(k)} = \mathbf{H}_k : \mathbf{E}_0$ the strain localization tensor of the phase k is identified as:

$$\mathbf{A}_k = \mathbf{H}_k : \left\langle \left(\mathbf{I} + \mathbf{C}_k : \mathbf{P}^{(k)}\right) : \mathbf{H}_k \right\rangle^{-1} \tag{A.19}$$

Using Eqs. (A.17) and (A.19) the strain localization coefficients A_k^v and A_k^d in Eqs. (15) and (16) are found.

The following section is dedicated to the evaluation of the coefficients H^v and H^d for the REV considered in this study.

A.2. Evaluation of strain localization parameters

This part is dedicated to the derivation of the elastic strain field in an infinite medium constituted of a 2-layered spherical inclusion, embedded with an imperfect interface, in a matrix subjected to uniform strain conditions at infinity. This solution is used to calculate the strain localization coefficients for the proposed micromechanical model. The considered model is presented in Fig. A.13. A spherical coordinate system (r, θ, ϕ) is used. The presentation of the equations follows the same steps as in the original formulations of Hervé and Zaoui [19] and their extension to consider imperfect interfaces by Ghabezloo [20], but in a relatively concise manner. The interested reader may refer to the original papers for more details.

Considering the isotropy and spherical symmetry of the model, the general solution can be obtained by superposing the solutions of two elementary problems: hydrostatic pressure and simple shear applied at infinity

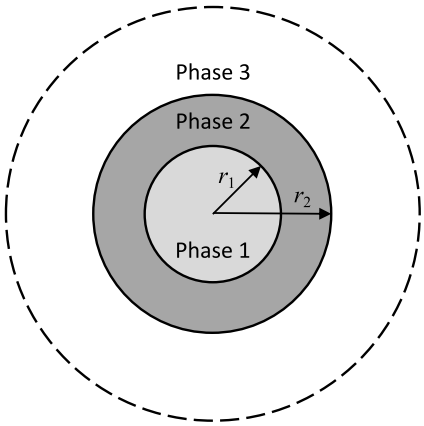

Fig. A.13. The 2-layered spherical inclusion embedded in an infinite matrix.

A.2.1. Hydrostatic pressure

A displacement in the following form is applied to the boundary of the model:

$$\underline{u}^0 = \frac{\theta_0}{3} r \underline{n} \tag{A.20}$$

where $\underline{n}$ is the outward normal vector to the boundary. Due to the spherical symmetry, the problem is one-dimensional. The solution of the displacement component u_r is given in each phase by the following form in which F_k and G_k ($k = 1, 2$) are constants which should be determined for each layer:

$$u_r^{(k)}(r) = F_k r + \frac{G_k}{r^2} \tag{A.21}$$

The non-zero components of the stress tensor are thus found to be:

$$\sigma_{rr}^{(k)} = 3k_k F_k - 4g_k \frac{G_k}{r^3} \tag{A.22}$$

$$\sigma_{\theta\theta}^{(k)} = \sigma_{\phi\phi}^{(k)} = 3k_k F_k + 2g_k \frac{G_k}{r^3} \tag{A.23}$$

The continuity of the radial stress and displacement at the interface between phases k and $k+1$ with radius r, considering a compliant interface given by the tensor $\mathbf{J}'_k$, implies that ($k = 1, 2$):

$$\left[\mathbf{J}_k\left(r_k\right) + \mathbf{J}'_k\left(r_k\right)\right]\mathbf{V}_k = \mathbf{J}_{k+1}\left(r_k\right)\mathbf{V}_{k+1} \tag{A.24}$$

where

$$\mathbf{V}_k = \left[F_k, G_k\right]^T; \quad \mathbf{J}_k(r) = \begin{bmatrix} r & \frac{1}{r^2} \\ 3k_k & -4\frac{g_k}{r^3} \end{bmatrix};$$

$$\mathbf{J}'_k(r) = \begin{bmatrix} 3k_k\eta_k^n & -\frac{4}{r^3}g_k\eta_k^n \\ 0 & 0 \end{bmatrix} \tag{A.25}$$

The relation between vectors $\mathbf{V}_{k+1}$ and $\mathbf{V}_k$ is given by:

$$\mathbf{V}_{k+1} = \mathbf{N}^{(k)}\mathbf{V}_k; \quad \mathbf{N}^{(k)} = \mathbf{J}_{k+1}^{-1}\left(r_k\right)\left[\mathbf{J}_k\left(r_k\right) + \mathbf{J}'_k\left(r_k\right)\right] \tag{A.26}$$

The vectors $\mathbf{V}_{k+1}$ are related to the vector $\mathbf{V}_k$ by:

$$\mathbf{V}_{k+1} = \mathbf{Q}^{(k)}\mathbf{V}_k; \quad \mathbf{Q}^{(k)} = \prod_{l=1}^{k} \mathbf{N}^{(l)} \tag{A.27}$$

Given that in the particular case of this research there only potentially exists an imperfect interface between phases 2 and 3 (HGMS and cement matrix), $\mathbf{J}'_k\left(r_k\right)$ will be a non-zero tensor only for $k = 2$, which stands for the contact between these phases:

$$\mathbf{N}^{(1)} = \begin{bmatrix} \frac{4g_2 + 3k_1}{4g_2 + 3k_2} & -\frac{4(g_1 - g_2)}{r_1^3(4g_2 + 3k_2)} \\ -\frac{3r_1^3(k_1 - k_2)}{4g_2 + 3k_2} & \frac{4g_1 + 3k_2}{4g_2 + 3k_2} \end{bmatrix} \tag{A.28}$$

$$\mathbf{N}^{(2)} = \begin{bmatrix} \dfrac{4g_3r_2 + 3k_2r_2 + 12g_3k_2\eta_2^n}{r_2\left(4g_3 + 3k_3\right)} & -\dfrac{4(g_2r_2 - g_3r_2 + 4g_2g_3\eta_2^n)}{r_2^4\left(4g_3 + 3k_3\right)} \\ \dfrac{3r_2^2(k_3r_2 - k_2r_2 + 3k_2k_3\eta_2^n)}{4g_3 + 3k_3} & \dfrac{4g_2r_2 + 3k_3r_2 - 12g_2k_3\eta_2^n}{r_2\left(4g_3 + 3k_3\right)} \end{bmatrix} \tag{A.29}$$

To avoid a singularity at $r = 0$, we should have $G_1 = 0$. Also, given the applied displacement at infinity, $F_3 = \dfrac{\theta}{3}$. It permits to find:

$$F_1 = \frac{1}{Q_{11}^{(2)}}F_3; \quad F_2 = \frac{Q_{11}^{(1)}}{Q_{11}^{(2)}}F_3 \tag{A.30}$$

$$G_2 = \frac{Q_{21}^{(1)}}{Q_{11}^{(2)}}F_3; \quad F_3 = \frac{Q_{21}^{(2)}}{Q_{11}^{(2)}}F_3 \tag{A.31}$$

A.2.2. Simple shear

New boundary displacements are applied for this condition, reading in spherical coordinates:

$$u_r^0 = \gamma r \sin^2\theta \cos 2\phi \tag{A.32}$$

$$u_\theta^0 = \gamma r \sin\theta \cos\theta \cos 2\phi \tag{A.33}$$

$$u_\phi^0 = -\gamma r \sin\theta \sin 2\phi \tag{A.34}$$

The displacement field in phase i is given by:

$$u_r^{(k)} = u_r^{(k)}(r) \sin^2\theta \cos 2\phi \tag{A.35}$$

$$u_\theta^{(k)} = U_\theta^{(k)}(r) \sin\theta \cos\theta \cos 2\phi \tag{A.36}$$

$$u_\phi^{(k)} = U_\phi^{(k)}(r) \sin\theta \sin 2\phi \tag{A.37}$$

where U_r, U_θ and U_ϕ, given below, are functions of r:

$$u_r^{(k)}(r) = A_k r - 6\frac{\nu_k}{1-2\nu_k}B_k r^3 + 3\frac{C_k}{r^4} + \frac{5-4\nu_k}{1-2\nu_k}\frac{D_k}{r^2} \tag{A.38}$$

$$U_\theta^{(k)}(r) = A_k r - \frac{7-4\nu_k}{1-2\nu_k}B_k r^3 - 2\frac{C_k}{r^4} + 2\frac{D_k}{r^2} \tag{A.39}$$

$$U_\phi^{(k)}(r) = -U_\theta^{(k)}(r) \tag{A.40}$$

Eqs. (A.35) to (A.40) represent the boundary displacement for the simple shear condition and the resulting displacement in each phase as a function of radius r. In these equations, the terms associated with the constants C_k and D_k are divided by the radius r. For phase 1, the initial value of the radius ($r = 0$) would lead to a singularity, so $C_1 = 0$ and $D_1 = 0$ to avoid this singularity. Moreover, in phase $n+1$ the radius tends to infinity, so the displacement values also tend to infinity, unless $B_{n+1} = 0$. Then $A_{n+1} = \gamma$, so it is possible to represent the displacement imposed in the boundary region by applying Eqs. (A.35) to (A.37) . The interface conditions between phases k and $k+1$ imply the continuity of $u_r, u_\theta, u_\phi, \sigma_{rr}, \sigma_{r\theta}, \sigma_{r\phi}$, but only four of these conditions are independent. The continuity conditions are written as:

$$\left[\mathbf{L}_k\left(r_k\right) + \mathbf{L}'_k\left(r_k\right)\right]\mathbf{W}_k = \mathbf{L}_{k+1}\left(r_k\right)\mathbf{W}_{k+1} \tag{A.41}$$

where

$$\mathbf{W}_k = \left[A_k, B_k, C_k, D_k\right]^T;$$

$$\mathbf{L}_k(r) = \begin{bmatrix} r & -\dfrac{6\nu_k}{1-2\nu_k}r^3 & \dfrac{3}{r^4} & \dfrac{5-4\nu_k}{1-2\nu_k}\dfrac{1}{r^2} \\ r & -\dfrac{7-4\nu_k}{1-2\nu_k}r^3 & -\dfrac{2}{r^4} & \dfrac{2}{r^2} \\ g_k & \dfrac{3\nu_k}{1-2\nu_k}g_k r^2 & -\dfrac{12}{r^5}g_k & \dfrac{2(\nu_k-5)}{1-2\nu_k}\dfrac{g_k}{r^3} \\ g_k & -\dfrac{7+2\nu_k}{1-2\nu_k}g_k r^2 & \dfrac{8}{r^5}g_k & \dfrac{2(1+\nu_k)}{1-2\nu_k}\dfrac{g_k}{r^3} \end{bmatrix} \tag{A.42}$$

and $\mathbf{L}'_k$ stands for the compliant interface between two phases and can be defined as:

$$\mathbf{L}'_k(r) = \begin{bmatrix} g_k\eta_k^n & \dfrac{3\nu_k}{1-2\nu_k}g_k r^2\eta_k^n & -\dfrac{12}{r^5}g_k\eta_k^n & \dfrac{2\left(\nu_k-5\right)}{1-2\nu_k}\dfrac{1}{r^3}g_k\eta_k^n \\ g_k\eta_k^t & \dfrac{7+2\nu_k}{1-2\nu_k}g_k r^2\eta_k^t & \dfrac{8}{r^5}g_k\eta_k^t & \dfrac{2\left(\nu_k+1\right)}{1-2\nu_k}\dfrac{1}{r^3}g_k\eta_k^t \\ 0 & 0 & 0 & 0 \\ 0 & 0 & 0 & 0 \end{bmatrix} \tag{A.43}$$

Once more, by considering the imperfect interface between phases 2 and 3 (HGMS and cement matrix), the tensor $\mathbf{L}'_k(r)$ will be not-zero only for the contact between them (i.e. $r = r_2$, $k = 2$). Then, the relationships between vectors $\mathbf{W}_{k+1}$ and $\mathbf{W}_k$ are given by:

$$\mathbf{W}_{k+1} = \mathbf{M}^{(k)}\mathbf{W}_k \quad ; \quad \mathbf{M}^{(k)} = \mathbf{L}_{k+1}^{-1}\left(r_k\right)\left[\mathbf{L}_k\left(r_k\right) + \mathbf{L}'_k\left(r_k\right)\right] \tag{A.44}$$

The vectors $\mathbf{W}_{k+1}$ are related to $\mathbf{W}_1$ by:

$$\mathbf{W}_{k+1} = \mathbf{P}^{(k)}\mathbf{W}_1 \quad ; \quad \mathbf{P}^{(k)} = \prod_{l=1}^{k}\mathbf{M}^{(l)} \tag{A.45}$$

As mentioned before, we have $C_1 = 0$, $D_1 = 0$, $B_3 = 0$ and $A_3 = \gamma$. Therefore we can obtain:

$$A_1 = \frac{P_{22}^{(2)}A_3}{P_{11}^{(2)}P_{22}^{(2)} - P_{12}^{(2)}P_{21}^{(2)}} \tag{A.46}$$

$$B_1 = -\frac{P_{21}^{(2)}A_3}{P_{11}^{(2)}P_{22}^{(2)} - P_{12}^{(2)}P_{21}^{(2)}} \tag{A.47}$$

and we can obtain W_2 as:

$$\mathbf{W}^{(2)} = \frac{A_3}{P_{22}^{(2)}P_{11}^{(2)} - P_{12}^{(2)}P_{21}^{(2)}}\mathbf{P}^{(1)}\begin{bmatrix} P_{22}^{(2)} \\ -P_{21}^{(2)} \\ 0 \\ 0 \end{bmatrix} \tag{A.48}$$

A.2.3. Average strains in phase k

When uniform strain conditions $\varepsilon_0 = \frac{\theta_0}{3}\mathbf{I} + \mathbf{e}_0$ apply at infinity, the following volume and deviatoric strains in each phase write as follows:

$$\bar{\theta}^{(k)} = \frac{F_k}{F_{n+1}}\bar{\theta}_0 \tag{A.49}$$

$$\bar{\mathbf{e}}^{(k)} = \frac{1}{A_{n+1}}\left[A_k - \frac{21}{5}\frac{r_k^5 - r_{k-1}^5}{\left(1-2\nu_k\right)\left(r_k^3 - r_{k-1}^3\right)}B_k\right]\bar{\mathbf{e}}_0 \tag{A.50}$$

By developing Eqs. (A.49) and (A.50) the following equations are obtained:

$$\bar{\theta}^{(1)} = \frac{\left(4g_2 + 3k_2\right)\left(4g_3 + 3k_3\right)}{X}\bar{\theta}_0 \tag{A.51}$$

$$\bar{\theta}^{(2)} = \frac{\left(4g_2 + 3k_1\right)\left(4g_3 + 3k_3\right)}{X}\bar{\theta}_0 \tag{A.52}$$

$$\bar{\theta}^{(3)} = \bar{\theta}_0 \tag{A.53}$$

$$X = \left(4g_2 + 3k_1\right)\left(4g_3 + 3k_2 + \frac{12g_3k_2\eta_2^n}{r_2}\right) + 3\left(k_1 - k_2\right)\left(4g_2 - 4g_3 + \frac{16g_2g_3\eta_2^n}{r_2}\right)\left(\frac{r_1}{r_2}\right)^3 \tag{A.54}$$

$$\bar{\mathbf{e}}^{(1)} = \frac{21P_{21}^{(2)}r_1^2 - 10\nu_1P_{22}^{(2)} + 5P_{22}^{(2)}}{\left(5 - 10\nu_1\right)\left(P_{11}^{(2)}P_{22}^{(2)} - P_{12}^{(2)}P_{21}^{(2)}\right)}\bar{\mathbf{e}}_0 \tag{A.55}$$

$$\bar{\mathbf{e}}^{(2)} = \frac{-\frac{P_{22}^{(2)}}{3}Y_1 - \frac{P_{21}^{(2)}}{2\nu_1 - 1}Y_2 + \frac{3\left(r_1^5 - r_2^5\right)}{5\left(r_1^3 - r_2^3\right)}P_{21}^{(2)}Y_3}{5g_2\left(P_{11}^{(2)}P_{22}^{(2)} - P_{12}^{(2)}P_{21}^{(2)}\right)\left(\nu_2 - 1\right)}\bar{\mathbf{e}}_0 \tag{A.56}$$

$$\bar{\mathbf{e}}^{(3)} = \bar{\mathbf{e}}_0 \tag{A.57}$$

$$Y_1 = 8g_1 + 7g_2 - 5\nu_2\left(2g_1 + g_2\right) \tag{A.58}$$

$$Y_2 = r_1^2\left[-7\left(g_1 - g_2\right) + 7\nu_2\left(2g_1 + g_2\right) + 3\nu_1\left(3g_1 - 24g_2\right)\right] \tag{A.59}$$

$$Y_3 = 7\left(g_1 + 4g_2\right) + 5\nu_1\left(g_1 - 8g_2\right) \tag{A.60}$$

If we replace the elastic properties of phase 1 with 0 (corresponding to the void space inside the hollow microsphere), we can obtain some reduced expressions of H_k^v and H_k^d for the REV considered in the lower part of Fig. 4.

$$\bar{\theta}^{(1)} = \frac{\left(4g_2 + 3k_2\right)\left(4g_3 + 3k_3\right)}{X}\bar{\theta}_0 \tag{A.61}$$

$$\bar{\theta}^{(2)} = \frac{4g_2\left(4g_3 + 3k_3\right)}{X}\bar{\theta}_0 \tag{A.62}$$

$$\bar{\theta}^{(3)} = \bar{\theta}_0 \tag{A.63}$$

$$X = 4g_2\left(4g_3 + 3k_2 + \frac{12g_3k_2\eta_2^n}{r_2}\right) - 3k_2\left(4g_2 - 4g_3 + \frac{16g_2g_3\eta_2^n}{r_2}\right)\left(\frac{r_1}{r_2}\right)^3 \tag{A.64}$$

$$\bar{\mathbf{e}}^{(1)} = \frac{21P_{21}^{(2)}r_1^2 + 5P_{22}^{(2)}}{5\left(P_{11}^{(2)}P_{22}^{(2)} - P_{12}^{(2)}P_{21}^{(2)}\right)}\bar{\mathbf{e}}_0 \tag{A.65}$$

$$\bar{\mathbf{e}}^{(2)} = \frac{P_{21}^{(2)}}{5\left(\nu_2 - 1\right)\left(P_{11}^{(2)}P_{22}^{(2)} - P_{12}^{(2)}P_{21}^{(2)}\right)}\left[\frac{P_{22}^{(2)}\left(5\nu_2 - 7\right)}{3P_{21}^{(2)}} + 7r_1^2\left(\nu_2 - 1\right) - \frac{84\left(r_1^5 - r_2^5\right)}{5\left(r_1^3 - r_2^3\right)}\right]\bar{\mathbf{e}}_0 \tag{A.66}$$

$$\bar{\mathbf{e}}^{(3)} = \bar{\mathbf{e}}_0 \tag{A.67}$$

Finally, having obtained the expressions of H_k^v and H_k^d, by considering Eq. (A.19) and recalling the definition of $\mathbf{C}_k = 3k_k\mathbf{J} + 2g_k\mathbf{K}$, it is possible to obtain $\mathbf{A}_k$ as shown in Eqs. (15) and (16). Thus, the homogenized parameters of the composite material can be obtained by using Eq. (1).

References

[1] E. Fjær, R. Holt, P. Horsrud, A. Raaen, R. Risnes, Petroleum Related Rock Mechanics, Elsevier Science, 2002, p. 514.

[2] E.B. Nelson, Well Cementing, Newnes, 1990.

[3] A. Anya, Lightweight and ultra-lightweight cements for well cementing - A review, Soc. Petrol. Eng. (2018) http://dx.doi.org/10.2118/190079-MS.

[4] T.M. Pique, F. Giurich, C.M. Martín, F. Spinazzola, D.G. Manzanal, Lightweight cement-based materials, in: P. Samui, D. Kim, N.R. Iyer, S. Chaudhary (Eds.), New Materials in Civil Engineering, Butterwort ed., Butterworth-Heinemann, 2020, pp. 565–589, http://dx.doi.org/10.1016/B978-0-12-818961-0.00016-8, arXiv:arXiv:1011.1669v3.

[5] S. Adjei, S. Elkatatny, Overview of the lightweight oil-well cement mechanical properties for shallow wells, J. Pet. Sci. Eng. 198 (2021) 108201, http://dx.doi.org/10.1016/j.petrol.2020.108201.

[6] A.S. Al-Yami, H.A. Nasr-El-Din, S.H. Al-Saleh, A. Al-Humaidi, C. Miller, H. Al-Yami, Y. El-Marsafawi, Long-term evaluation of low-density cement: Laboratory studies and field application, Soc. Petrol. Eng. (2007) SPE–105340–MS, http://dx.doi.org/10.2118/105340-MS.

[7] X. Yao, S.D. Hua, U. Nanjng, Design of a novel composite agent for improving the toughness of oil w ell cement sheath, Soc. Petrol. Eng. (2007) http://dx.doi.org/10.2118/106010-MS.

[8] P. Singh, M.P. Sinha, K. Lal, S.K. Malhotra, P. Kumar, Stress modelling and design of elastic cement system to withstand well-bore pressure during hydro-fracturing and casing integrity testing. stress modeling, Soc. Petrol. Eng. (2017) http://dx.doi.org/10.2118/185402-MS.

[9] Y. Yan, Z. Guan, W. Yan, H. Wang, Mechanical response and damage mechanism of cement sheath during perforation in oil and gas well, J. Pet. Sci. Eng. 188 (2020) 106924, http://dx.doi.org/10.1016/j.petrol.2020.106924.

[10] L. Dormieux, D. Kondo, F.-J. Ulm, Microporomechanics, John Wiley & Sons Inc, 2006.

[11] A. Zaoui, Continuum micromechanics: survey, J. Eng. Mech. 128 (8) (2002) 808–816.

[12] O. Bernard, F.-J. Ulm, E. Lemarchand, A multiscale micromechanics-hydration model for the early-age elastic properties of cement-based materials, Cem. Concr. Res. 33 (9) (2003) 1293–1309.

[13] F.-J. Ulm, G. Constantinides, F.H. Heukamp, Is concrete a poromechanics material? - A multiscale investigation of poroelastic properties, Mater. Struct. 37 (265) (2004) 43–58, http://dx.doi.org/10.1617/14100.

[14] J. Sanahuja, L. Dormieux, G. Chanvillard, Modelling elasticity of a hydrating cement paste, Cem. Concr. Res. 37 (10) (2007) 1427–1439, http://dx.doi.org/10.1016/j.cemconres.2007.07.003.

[15] S. Ghabezloo, Association of macroscopic laboratory testing and micromechanics modelling for the evaluation of the poroelastic parameters of a hardened cement paste, Cem. Concr. Res. 40 (8) (2010) 1197–1210.

[16] S. Ghabezloo, Effect of the variations of clinker composition on the poroelastic properties of hardened class G cement paste, Cem. Concr. Res. 41 (8) (2011) 920–922.

[17] S. Ghabezloo, Micromechanics analysis of thermal expansion and thermal pressurization of a hardened cement paste, Cem. Concr. Res. 41 (5) (2011) 520–532.

[18] B. Pichler, C. Hellmich, Upscaling quasi-brittle strength of cement paste and mortar: A multi-scale engineering mechanics model, Cem. Concr. Res. 41 (5) (2011) 467–476, http://dx.doi.org/10.1016/j.cemconres.2011.01.010.

[19] E. Herve, A. Zaoui, n-Layered inclusion-based micromechanical modelling, Internat. J. Engrg. Sci. 31 (1993) 1–10, http://dx.doi.org/10.1016/0020-7225(93)90059-4.

[20] S. Ghabezloo, A micromechanical model for the effective compressibility of sandstones, Eur. J. Mech. A Solids 51 (2015) 140–153, http://dx.doi.org/10.1016/j.euromechsol.2014.12.007.

[21] C. Martín, N. Scarponi, Y. Villagrán, D. Manzanal, T. Piqué, Pozzolanic activity quantification of hollow glass microspheres, Cem. Concr. Compos. 118 (2021) 103981, http://dx.doi.org/10.1016/j.cemconcomp.2021.103981.

[22] R.C. Smith, C.A. Powers, T.A. Dobkins, New ultra-lightweight cement with super strength, JPT, J. Petrol. Technol. 32 (8) (1980) 1438–1444, http://dx.doi.org/10.2118/8256-pa.

[23] M. Lanzón Torres, P.A. García-Ruiz, Lightweight pozzolanic materials used in mortars: Evaluation of their influence on density, mechanical strength and water absorption, Cem. Concr. Compos. 31 (2009) 114–119, http://dx.doi.org/10.1016/j.cemconcomp.2008.11.003.

[24] C. Mata, A. Calubayan, Use of hollow glass spheres in lightweight cements - Selection criteria, Soc. Petrol. Eng. (2016) 25–27, http://dx.doi.org/10.2118/182399-ms.

[25] L. Wang, F. Aslani, I. Hajirasouliha, E. Roquino, Ultra-lightweight engineered cementitious composite using waste recycled hollow glass microspheres, J. Clean. Prod. 249 (2020) 119331, http://dx.doi.org/10.1016/j.jclepro.2019.119331.

[26] M.N. Abdullah, D. Bedford, S.R. Wong, H.S. Yap, Prehydrating high-strength microspheres in lightweight cement slurry creates value for offshore Malaysian operator, Soc. Petrol. Eng. (2013) 1–9, http://dx.doi.org/10.2118/165796-ms.

[27] J. Eshelby, The determination of the elastic field of an ellipsoidal inclusion, and related problems, Proc. R. Soc. Lond. Ser. A Math. Phys. Eng. Sci. (1957) 376–396.

[28] M. Königsberger, B. Pichler, C. Hellmich, Multiscale poro-elasticity of densifying calcium-silicate hydrates in cement paste: An experimentally validated continuum micromechanics approach, Internat. J. Engrg. Sci. 147 (2020) 103196, http://dx.doi.org/10.1016/j.ijengsci.2019.103196.

[29] S. Bahafid, S. Ghabezloo, M. Duc, P. Faure, J. Sulem, Effect of the hydration temperature on the microstructure of class G cement: C-S-H composition and density, Cem. Concr. Res. 95 (2017) 270–281, http://dx.doi.org/10.1016/j.cemconres.2017.02.008.

[30] S. Bahafid, S. Ghabezloo, P. Faure, M. Duc, J. Sulem, Effect of the hydration temperature on the pore structure of cement paste: Experimental investigation and micromechanical modelling, Cem. Concr. Res. 111 (September 2017) (2018) 1–14, http://dx.doi.org/10.1016/j.cemconres.2018.06.014.

[31] W. Wilson, J. Rivera-Torres, L. Sorelli, A. Durán-Herrera, A. Tagnit-Hamou, The micromechanical signature of high-volume natural pozzolan concrete by combined statistical nanoindentation and SEM-EDS analyses, Cem. Concr. Res. 91 (2017) 1–12.

[32] L. Yu, S. Zhou, W. Deng, Properties and pozzolanic reaction degree of tuff in cement-based composite, Adv. Concr. Constr. 3 (2015) 71–90, http://dx.doi.org/10.12989/acc.2015.3.1.071.
[33] Y. Benveniste, The effective mechanical behaviour of composite materials with imperfect contact between the constituents, Mech. Mater. 4 (2) (1985) 197–208, http://dx.doi.org/10.1016/0167-6636(85)90016-X.
[34] J. Qu, The effect of slightly weakened interfaces on the overall elastic properties of composite materials, Mech. Mater. 14 (4) (1993) 269–281, http://dx.doi.org/10.1016/0167-6636(93)90082-3.
[35] Y. Wu, Z. Ling, Z. Dong, Stress-strain fields and the effectiveness shear properties for three-phase composites with imperfect interface, Int. J. Solids Struct. 37 (9) (2000) 1275–1292, http://dx.doi.org/10.1016/S0020-7683(98)00295-9.
[36] Z. Hashin, Thin interphase/imperfect interface in elasticity with application to coated fiber composites, J. Mech. Phys. Solids 50 (12) (2002) 2509–2537, http://dx.doi.org/10.1016/S0022-5096(02)00050-9.
[37] K. Yanase, J.W. Ju, Effective elastic moduli of spherical particle reinforced composites containing imperfect interfaces, Int. J. Damage Mech. 21 (1) (2011) 97–127, http://dx.doi.org/10.1177/1056789510397076.
[38] C.M. Sayers, M.L. Kachanov, Microcrack-induced elastic wave anisotropy of brittle rocks, J. Geophys. Res. 100 (B3) (1995) 4149–4156, http://dx.doi.org/10.1029/94JB03134.
[39] J. Qu, M. Cherkaoui, Fundamentals of Micromechanics of Solids, Wiley, 2006, p. 400.
[40] American Petroleum Institute, API 10A: Cements and Materials for Well Cementing, Twenty fifth ed., 2019.
[41] American Petroleum Institute, API 10B-2: Recommended practice for testing well cements, second ed., 2013.
[42] M.I. ul Hassan, B. Pichler, R. Reihsner, C. Hellmich, Elastic and creep properties of young cement paste, as determined from hourly repeated minute-long quasi-static tests, Cem. Concr. Res. 82 (2016) 36–49.
[43] E. Binder, M. Königsberger, R. Díaz Flores, H.A. Mang, C. Hellmich, B.L. Pichler, Thermally activated viscoelasticity of cement paste: Minute-long creep tests and micromechanical link to molecular properties, Cem. Concr. Res. 163 (2023) 107014.
[44] A. Zaoui, Continuum micromechanics: survey, J. Eng. Mech. - ASCE 128 (8) (2002) 808–816, http://dx.doi.org/10.1061/(ASCE)0733-9399(2002)128:8(808).
[45] R.J. Eagan, J.C. Swearekgen, Effect of composition on the mechanical properties of aluminosilicate and borosilicate glasses, J. Am. Ceram. Soc. 61 (1–2) (1978) 27–30.
[46] T. Rouxel, Elastic properties and short-to medium-range order in glasses, J. Am. Ceram. Soc. 90 (2007) 3019–3039.
[47] C. Campañá, B.N.J. Persson, M.H. Müser, Transverse and normal interfacial stiffness of solids with randomly rough surfaces, J. Phys.: Condens. Matter 23 (8) (2011) 085001, http://dx.doi.org/10.1088/0953-8984/23/8/085001.
[48] J. White, Underground Sound - Application of Seismic Waves, Elsevier Science Publishing Co., 1983.